Hydroperoxide and carboxyl groups preferential location in oxidized biomembranes experimentally determined by small angle X-ray scattering: Implications in membrane structure

Structural characterization of oxidized lipid membranes by small angle X-ray scattering promotes a better understanding of oxidized groups location

Raffaela De Rosa[a], Francesco Spinozzi[b,*], Rosangela Itri[a,**]

[a] *Institute of Physics, University of Sao Paulo, SP, Brazil*
[b] *Department of Life and Environmental Sciences, Polytechnic University of Marche, Ancona, Italy*

Keywords:

Abstract

The comprehension at molecular level of the structural changes promoted on cell membranes due to the presence of oxidized lipid species in the lipid bilayer is of paramount importance. Here, we consider small angle X-Ray scattering (SAXS) data from model membranes (large unilamellar vesicles, LUVs) composed of 1-palmitoyl-2-oleoyl-*sn*-glycero-3-phosphocoline (POPC) and two oxidized species, namely its hydroperoxidized form POPC-OOH and 1-palmitoyl-2-azelaoyl-*sn*-glycero-3-phosphocholine (PazePC) lipid that has a carboxyl group at the end of its truncated *sn*-2 chain. The replacement of POPC by either POPC-OOH (POPC-OOH$_x$POPC$_{1-x}$) or PazePC (PazePC$_x$POPC$_{1-x}$), with oxidized lipid molar ratio x varying from 0.00 up to 1.00, permits to inspect changes in the membrane structural properties due to oxidation. The volume fraction distribution of each lipid chemical group along the bilayer was retrieved from the SAXS curves. The results demonstrate in a quantitative manner that 95% of the hydroperoxide group lies in the membrane polar moiety, near the carbonyl and phosphate groups, probably forming H-bonds, whereas just 5% of OOH group experiences the polar/apolar interface, for all values of x studied. On the other hand, in the case of PazePC up to $x = 0.33$, the carboxyl group presents a bimodal distribution in the interior and polar regions of the oxidized lipid membrane, probably due to a dynamic movement of the shortened alkyl chain towards the water interface. Noteworthy, the mean molecular area A gradually increases from 65.4 ± 0.4 Å^2 for POPC bilayers to 78 ± 2 Å^2 for pure POPC-OOH bilayers, whereas POPC-OOH membrane thickness resulted to be 20% thinner than the non-oxidized POPC membrane. In the case of PazePC up to $x = 0.33$, A increases to 67 ± 2 Å^2 with 10% of membrane thinning. Taken together, our SAXS experimental results unravel how the oxidation progress affects the membrane structural features, thus paving the way to better comprehend membrane damage under oxidative stress.

*Corresponding author: f.spinozzi@univpm.it
**Corresponding author: itri@if.usp.br

1. Introduction

Lipids of biological membranes are prone to chemical and photo-induced oxidation because they contain high amounts of monounsaturated and polyunsaturated fatty acids. By turn, lipid oxidation leads to the formation of new molecular entities, which resemble lipids but have hydrophilic groups hanging on the alkyl chains or often on the shortened acyl oxidized lipid tails [1].

A controlled amount of oxidized lipid products (referred to herein as OxL) is required for cell signaling, maturation and differentiation, as well as apoptosis. However, the production of OxL, if uncontrolled, can have a deleterious effect on the functioning of the cell, and also be involved in a variety of diseases [2, 3]. Indeed, methodological advances at the molecular-level detection and identification of oxidative species have provided insights into oxidative lipid modification and its involvement in cell signaling as well as in major diseases and inflammation processes [4, 5, 6, 7, 8]. Extensive evidence suggests a correlation between lipid peroxidation and degenerative neurological disorders such as Parkinson's and Alzheimer's diseases [9, 10, 11], as well as type 2 diabetes [12, 13]. Aging and carcinogenesis induced by UV and many physiological processes have been also related to the formation of oxidative species [14, 5, 12]. However, in spite of the obvious relevance of understanding the molecular basis of several diseases, the exact modes of action of oxidized lipids on membranes remain elusive.

Usually, lipid oxidation reactions start with lipid hydroperoxide formation and progress to lipids with truncated alkyl chains [15]. Several molecular dynamics (MD) studies have been carried out during the last decade (reviewed by Jurkiewicz et al. [16] and more recently by Siani et al. [1]) with different oxidized lipid species inside the model lipid bilayer systems. In particular, simulations results show for hydroperoxized lipids an increase in membrane lateral area accompanied by a decrease in the bilayer thickness and order parameters [17, 1, 18]. The presence of hydroperoxide groups in the lipid bilayer does not promote pore formation regardless of the water model and force field employed. However, there is a controversy in the literature concerning he hydroperoxized group location in the membrane predicted by MD. Some MD results point out that hydroperoxized groups of OxL tend to be preferentially located near the headgroup region [17, 19, 1], whereas bimodal distribution of the hydroperoxized group in the membrane interior and polar moiety has also been reported [18]. Theferefore, results from computing simulations are not unique in terms of hydroperoxized group location in the lipid bilayer but, in fact, depend on the used force field and methodology approach.

From the experimental point of view, results using giant unilamellar vesicles (GUVs) as model membranes revealed that the hydroperoxide groups (Figure 1) have a significant impact on membrane features as, for instance, increase in lateral area [20] in good agreement with MD data, fluidity [21], elastic modulus [22] and rafts organization [23]. On the other hand, there is not any direct experimental evidence regarding the lipid bilayer thickness decrease or the location of the hydroperoxide group inside the membrane.

Subsequent oxidation leading to lipids with shortened chains also alters membranes' properties and may lead to an increase in membrane permeability, pores formation [24, 25]

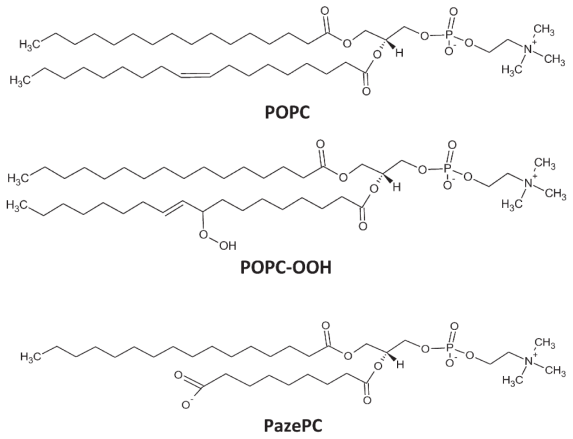

Figure 1: Chemical structures of 1-palmitoyl-2-oleoyl-*sn*-glycero-3-phosphocholine (POPC) and two oxidatively modified phospholipids: the hydroperoxidized form of POPC (POPC-OOH) and 1-palmitoyl-2-azelaoyl-*sn*-glycero-3-phosphocholine (PazePC).

and membrane rupture [26]. Khandelia and Mouritsen [27] simulated a system comprising 1-palmitoyl-2-azelaoyl-*sn*-glycero-3-phosphocholine (PazePC) lipid that has a carboxylate group at the end of its truncated *sn*-2 chain (Figure 1). According to MD results, the shortened tail of PazePC completely reverses orientation, thus exposing its carboxyl group to aqueous phase, in very good agreement with Förster-type resonance energy transfer (FRET) results obtained between cytochrome-c and fluorescently labeled PazePC model membranes [28] and electron density profiles extracted from X-ray reflectivity on supported lipid bilayers containing up to 20 mol % of PazePC [29]. Interestingly, PazePC may have implication in atherogenesis [30].

Therefore, either as a result of a physiological process or derived from photo-oxidation, the influence of OxL on the physical properties of membrane is not fully understood. In fact, the complexity of the studied processes and the limitations of the tools necessary to characterize the membrane structural modifications imposed by the presence of OxL hinder our current understanding of this phenomenon. Therefore, in spite of the fact that MD can describe qualitatively some lipid bilayer properties, it is imperative the use of proper experimental techniques to access structural information from membranes in a quantitative manner. On this ground, small angle X-Ray scattering (SAXS) technique is a powerful tool to investigate lipid bilayer structure. In particular, the experimental determination of the volume fraction distribution of each chemical group of the lipid molecules along the bilayer has been obtained by analyzing SAXS data with the well-known scattering density profile (SDP) model[31, 32, 33, 34, 35, 36], which we have modified and entered in the Genfit software data analysis package [37]. Specifically, SAXS curves of different mixtures of lipids are jointly analyzed by refining common structural parameters. Here, we take advantage of SDP model to obtain the preferential sites of oxidized groups inside the membrane from SAXS data. Our experimental approach consists in incorporating oxidized phospholipid species into the vesicles bilayer. They are: POPC-OOH, the hydroperoxidized form

of 1-palmitoyl-2-oleoyl-*sn*-glycero-3-phosphocholine (POPC), and PazePC (Figure 1). By replacing defined amounts of the unsaturated lipid with a corresponding oxidized product, the oxidation process can be mimicked, yielding vesicles of varying oxidized lipid concentration. Understanding and measuring how oxidation of the lipid bilayer affects its structural architecture is key to comprehend how it impacts on cell destabilization and damage.

2. Materials and Methods

2.1. Materials

The phospholipids POPC and PazePC were purchased from Avanti Polar Lipids. POPC-OOH was synthesized by our group according to the protocol described elsewhere [38]. Figure 1 shows the chemical structures of POPC, POPC-OOH and PazePC.

2.2. Large unilamellar vesicles (LUVs) preparation

The investigated LUVs consisted of $POPC_{1-x}$POPC-OOH_x (with the oxidized lipid molar ratio $x = 0.00$, 0.33, 0.67 and 1.00) and $POPC_{1-x}PazePC_x$ (with $x = 0.00$, 0.10 and 0.33), respectively. The lipids mixtures were dissolved in chloroform, which was evaporated under N_2 stream, to deposit a thin lipid film on the wall of a glass tube. The final traces of residual solvent were removed under vacuum at room temperature for 1 h. 10 mM of total lipids for each LUV composition were suspended in ultra-pure Milli-Q water, followed by extrusion through two-stacked polycarbonate membranes of 100 nm diameter pores (Mini-Extruder system, Avanti Polar Lipids Inc, Alabaster, Alabama, USA). This process was repeated 31 times, and the LUVs dimension (100 nm) was checked by dynamic light scattering (DLS). All liposomal preparations were freshly prepared and used in the same day. Of note, samples prepared with molar ratio of PazePC larger than 0.33 were not characterized as LUVs by both SAXS and DLS and, hence, discarded from our data analysis.

2.3. Small angle X-ray scattering (SAXS)

SAXS experiments were performed at the Brazilian Synchrotron Light Laboratory (LNLS, Campinas, Brazil). The scattering vector modulus $q = 4\pi \sin\theta/\lambda$ (2θ being the scattering angle and λ the X-ray wavelength fixed to 1.548 Å) ranged from 0.012 and 0.453 $Å^{-1}$. All experiments were carried out at room temperature of $22 \pm 1°C$.

SAXS data analysis was based on the SDP model that has been successfully applied to extract from MD simulations of lipid bilayers the number densities and hence the volume fraction distributions of the different chemical groups along the bilayer normal [39, 36]. Since X-ray or neutron scattering length densities (SLDs) can be easily calculated from volume fraction distributions, the same model has also been exploited to analyze SAXS as well as small-angle neutron scattering (SANS) data of lipid bilayers. The basic concept of the model is to describe the volume fraction distribution of lipid chemical groups with elementary analytic functions, such Gaussians and error functions. The water volume fraction distribution is then obtained as the complement to unity with respect to the total lipid volume fraction. However, since the volume fraction distribution profile of CH_2, which is the dominant hydrophobic group, is hardly described by a single Gaussian, a different strategy

is followed. Firstly, it the total volume fraction distribution of all hydrophobic groups is defined and modeled by an error function that decreases from one to zero on going from the center of the bilayer to the polar head. The midpoint of this transition defines the monolayer hydrophobic thickness D_{hyd}, corresponding to the Gibbs surface dividing the apolar/polar interface. Secondly, the volume fraction distribution of CH_2 is taken as the difference between the error function and the Gaussian profiles describing all the other hydrophobic groups.

In order to extend the application of the SDP model to more complex lipid molecular architectures or to lipid mixtures, we have considered that the description of the volume fraction distribution with a single Gaussian peak is a too simple view. A possible alternative, which however preserves the mathematical tractability of the Gaussian, is to describe the volume fraction distribution of each i-chemical group (apart CH_2) along the axis z perpendicular to the bilayer plane by the following combination of two error functions,

$$E_2(z, z_i, w_i, \sigma_i) = \frac{1}{2}\left[\mathrm{erf}\left(\frac{z - z_i + w_i}{2^{1/2}\sigma_i}\right) - \mathrm{erf}\left(\frac{z - z_i - w_i}{2^{1/2}\sigma_i}\right)\right] \quad (1)$$

where z_i denotes the peak position, $2w_i$ is the peak width and σ_i (the error function standard deviation) represents the peak smoothness. Two peaks at symmetrical positions $\pm z_i$ based on the previous function are defined by

$$E_{2s}(z, z_i, w_i, \sigma_i) = E_2(z, z_i, w_i, \sigma_i) + E_2(z, -z_i, w_i, \sigma_i) \quad (2)$$

A representative plot of $E_{2s}(z, z_i, w_i, \sigma_i)$ is reported in Figure S1 in the Supporting Information. The set of all N groups are numbered so that the first N_{hyd} groups are the hydrophobic ones, the other N_{pol} are polar groups and the last one is water. The first group is always the most abundant hydrophobic species, typically CH_2. It can be shown that the volume fraction distribution of the i-group is

$$\varphi_i(z) = \frac{\mathrm{n}_i \nu_i}{A} \frac{E_{2s}(z, z_i, w_i, \sigma_i)}{2w_i} \quad (3)$$

where ν_i is the molecular volume of the i-group, n_i is the number of i-groups in the lipid molecule and $A = V_{\mathrm{hyd}}/D_{\mathrm{hyd}}$ is the area per molecule, $V_{\mathrm{hyd}} = \sum_{i=1}^{N_{\mathrm{hyd}}} \mathrm{n}_i \nu_i$ being the total hydrophobic volume. To note, according to Kučerka et al. [33], the volume fraction of the total hydrophobic part of the lipid is $\varphi_{\mathrm{hyd}}(z) = E_2(z, 0, D_{\mathrm{hyd}}, \sigma_{\mathrm{hyd}})$ and the water volume fraction is

$$\varphi_N(z) = 1 - \varphi_{\mathrm{hyd}}(z) - \sum_{i=N_{\mathrm{hyd}}+1}^{N-1} \varphi_i(z) \quad (4)$$

where the sum runs over the polar groups. The SLD of the bilayer is $\rho(z) = \sum_{i=1}^{N} \varphi_i(z) b_i/\nu_i$, where b_i is the scattering length of the group corresponding, for SAXS, to the number of electrons carried on by the group multiplied by the classical radius of the electron ($r_{\mathrm{e}} =$

$0.28 \cdot 10^{-12}$ cm). The Fourier transform of the excess SLD can be calculated up to the maximum hydrated monolayer length D, $F(q) = 2\int_0^D [\rho(z) - \rho_0]\cos(qz)dz$, where ρ_0 is the SLD of the bulk solvent and $D = \max(\{z_i + w_i + p\sigma_i\})$, with $p \approx 3$. As a result, we following analytic function is obtained

$$\begin{aligned} F(q) &= \frac{2}{A}\sum_{i=2}^{N_{\rm hyd}}(\rho_i - \rho_1)\mathrm{n}_i\nu_i\cos(qz_i)\frac{\sin(qw_i)}{qw_i}e^{-q^2\sigma_i^2/2} \\ &+\frac{2}{A}\sum_{i=N_{\rm hyd}+1}^{N_{\rm hyd}+N_{\rm pol}}(\rho_i - \rho_N)\mathrm{n}_i\nu_i\cos(qz_i)\frac{\sin(qw_i)}{qw_i}e^{-q^2\sigma_i^2/2} \\ &+2(\rho_1 - \rho_N)D_{\rm hyd}\frac{\sin(qD_{\rm hyd})}{qD_{\rm hyd}}e^{-q^2\sigma_{\rm hyd}^2/2} \\ &+2(\rho_N - \rho_0)D\frac{\sin(qD)}{qD}. \end{aligned} \quad (5)$$

Some properties of the modified SDP model (MSDP) with respect to the standard version deserve to be underlined. Firstly, the SLD of the water in contact with the lipid molecule, ρ_N, could be different from the one of the solvent. Secondly, the volume fraction peak of each group is defined by three adjustable parameters, z_i, w_i and σ_i instead of the two parameters z_i and σ_i of a Gaussian peak. Although, from one side, this feature leads to an increase of the total number of parameters, on the other side it can easily adapt to the simple but widely accepted description of the lipid molecule as constituted by only two or three groups (tipically head, core and tail), each one with almost constant SLD, as shown in Figure S2 in the Supporting Information.

The "macroscopic differential scattering cross section", simply referred to as the scattering intensity, provided by a SAXS experiment is finally expressed by the equation

$$\frac{d\Sigma}{d\Omega}(q) = \frac{c_V}{D_B}\frac{2\pi}{q^2}F^2(q) \quad (6)$$

where D_B is the Luzzati thickness (Figure S2 in the Supporting Information), $D_B = 2(V_{\rm pol} + V_{\rm hyd})/A$ ($V_{\rm pol} = \sum_{i=N_{\rm hyd}+1}^{N-1}\mathrm{n}_i\nu_i$ being the total lipid polar volume) and c_V is the total volume fraction of the dry lipid, $c_V = C\,N_A(V_{\rm pol} + V_{\rm hyd})$ (C and N_A are the molar lipid concentration and Avogadro's number, respectively).

When the model is intended to be applied to the analysis of a batch of SAS curves recorded on samples with similar chemical-physical conditions (e.g. different mixtures of the same lipid molecules), more stable and robust results can be obtained by adopting a global-fit strategy, where some fitting parameters that in principle should not vary for the different samples (such as molecular volumes of groups) are treated as common parameters, whereas other fitting parameters are curve-specific, being dependent on the particular experimental conditions investigated. The global-fit concept can be also extended to the simultaneous analysis of two or more batches of SAS data (for example a series of mixtures of a lipid L_1 with a lipid L_2 and an other series of mixtures of the same lipid L_1 and a

third lipid L_3), when at least a common fitting parameter can be defined. Moreover, when the number of curve-specific fitting parameters of the b-batch of curves is quite large and hence many combinations of them can adequately fit the data, it is recommended to exploit a regularization procedure [40, 41], based on the determination of the damping term F_b of the batch defined on the basis of the relative squared difference of two curve-specific fitting parameters, $X_{i,j}$ and $X_{i+1,j}$, which refer to SAS curves of samples with the closest chemical-physical conditions,

$$F_b = \sum_{i=1}^{K_b} \sum_{j=1}^{P_b-1} (X_{i+1,j}/X_{i,j} - 1)^2. \quad (7)$$

Notice indeed that in Equation 7, the index i runs over the K_b experimental conditions of a series, ordered on the basis of a composition coefficient, e.g. molar fraction or molar concentration, being j the index of the P_b parameters that have been chosen to be under the regularization constraint. The overall merit function to be minimized by the global-fit analysis is then $\mathcal{H} = \chi^2 + \sum_b \alpha_b F_b$, where χ^2 is the average standard reduced chi-square of all the N_c experimental SAS curves $I_{\exp_c}(q_i)$ with their standard deviation $\sigma_c(q_i)$, according to $\chi^2 = (1/N_c)\sum_c \chi_c^2$, with $\chi_c^2 = (1/N_q)\sum_i \sigma_c(q_i)^{-2}[I_{\exp_c}(q_i) - \kappa\frac{d\Sigma}{d\Omega}(q_i) - B]^2$. The damping function weights α_b are wisely chosen so that the value of $\sum_b \alpha_b F_b$ at the end of the minimization does not exceed approximately 10% of χ^2. The scaling factor κ and the background B have been added in order, respectively, to refine possible mistakes in the instrumental calibration and to take into account incoherent scattering effects, which are quite relevant in case of SANS.

Table 1: List of all chemical groups and their molecular volumes, molecular weights, electron numbers, and compositions in the three lipid molecules investigated. According to Kučerka et al. [33], the combined groups are: the carbonyl + glycerol (CG), the phosphate + CH_2CH_2N (PCN), and the three CH_3 of the choline ($CholCH_3$). The oxidized groups from POPC-OOH and from PazePC are the unsaturated CHCH + hydroperoxide CHOOH (PX) and the dissociated carboxylate COO^- (CX), respectively. [(a)]Standard literature data [42].

i-group	ν_i[(a)] ($Å^3$)	M_i ($g\,mol^{-1}$)	Z_i (q_e)	n_i - POPC	n_i - POPC-OOH	n_i - PazePC
CH_2	27.7	14.03	8	28	27	21
CH_3	52.9	15.04	9	2	2	1
CH	21.5	13.02	7	2		
CG	143.3	129.09	67	1	1	1
PCN	87.8	137.03	70	1	1	1
$CholCH_3$	99.9	45.11	27	1	1	1
PX	94.8	72.03	38		1	
CX	51.0	44.01	23			1
H_2O	29.9	18.02	10			

The determination of the standard deviation of each fitting parameter is carried on by repeating several times (typically 10-20 times) the global-fit analysis by randomly sampling,

for each repetition, the experimental intensities $I_{\exp_c}(q_i)$ for any q_i-channel within the Gaussian distribution defined by the experimental SAS uncertainty $\sigma_c(q_i)$. The minimization of the merit functional $\mathcal{H}$ is performed by a combination of the Simulated Annealing and the Simplex methods. The MSDP model, with all the features here described, can be applied by using the recently updated Genfit software [37].

3. Results

Two batches of binary mixtures of POPC, POPC:POPC-OOH and POPC:PazePC, have been prepared, as described in the Materials and Methods. The chemical groups constituting the lipids and the bulk water are defined and listed in Table 1, along with their main properties and their number n_i in each of the three lipid molecules.

SAXS curves of the two batches, recorded in two different experimental campaigns at the LNLS synchrotron for the mixtures POPC:POPC-OOH and POPC:PazePC, respectively, are reported in Figure 2 in semilogarithmic form and in Figure S3 in the Supporting Information in the form of $q\sqrt{\frac{d\Sigma}{d\Omega}(q)}$ vs. q to emphasize the differences.

At a first glance, the trend of the curves in Figure 2 is quite similar, with the presence of a large band centered at $q \approx 0.12$ Å^{-1}, which is typical of almost flat bilayer sheets [43]. In all cases, the band is preceeded by a the deep minimum that reaches more or less the same value of the intensity at the highest q, indicating the absence of lipid domains or pores in the bilayer sheets [44]. As a consequence, since the two SAXS datasets suggest that both mixtures are basically homogeneous, the MSDP model, previously introduced, can be applied by considering as *lipid units* $POPC_{1-x}POPC\text{-}OOH_x$ (with $x = 0.00$, 0.33, 0.67 and 1.00) and $POPC_{1-x}PazePC_x$ (with $x = 0.00$, 0.10 and 0.33), respectively. Clearly, on the basis of x, for each investigated sample it is straightforward to fix the number of chemical groups that form the lipid unit (Table 1).

We notice that there are undoubtly three hydrophobic groups (CH_2, CH_3 and CH) and three polar groups (CG, PCN and $CholCH_3$) in the lipid membrane structure. Moreover, since there is no experimental evidence regarding the location inside the lipid bilayer of the "extended" hydroperoxide group of POPC-OOH (referred to PX herein, which includes also the two close unsaturated carbons CHCH) and the carboxylate group of PazePC (refferred to as CX herein), we have considered that it is possible to find these groups in the hydrophobic core as well as in the polar head region. In this way, a fourth hydrophobic group (referred to as PX_{hyd} or CX_{hyd}) and a fourth polar group (PX_{pol} or CX_{pol}) were also taken into account. Accordingly, we define x_{pol} as the fraction of the total number of oxidized group (X = PX or X = CX) that experiences the polar region.

By doing so, both batches of SAXS curves have been simultaneously fitted to the MSDP model by the global-fit strategy shown in Materials and Methods. Fitting parameters, reported in Table 2, have been organized in three classes, truly common-parameters (they assume the same value for any curve of the two batches), batch-parameters (the same value of any curve of the same batch) and curve-specific parameters.

The first class includes the molecular volumes of methylene, ν_{CH_2}, phosphatidylcholine, $V_{PC} = \nu_{CG} + \nu_{PCN} + \nu_{CholCH_3}$, and bulk water, ν_{H_2O}, together with the volume ratios in

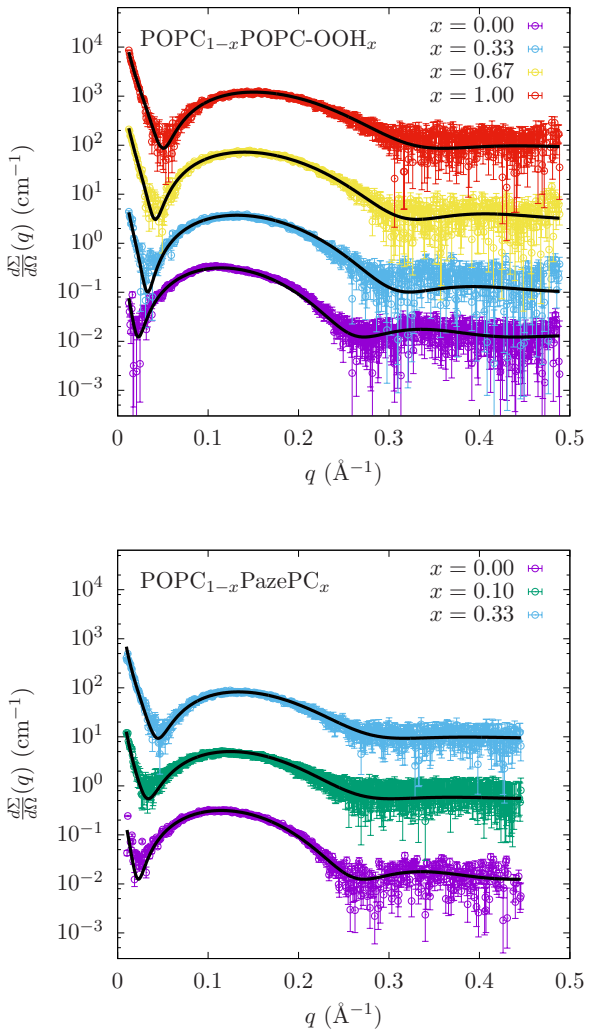

Figure 2: SAXS curves of POPC:POPC-OOH (top panel) and POPC:PazePC (bottom panel) mixtures. Points represent the experimental curves divided by the optimum scaling factor κ obtained by the global-fit analysis of both batches on the basis of the MSDP model. Solid black lines are the best-fit curves. All curves are stacked by a factor 20 for the sake of clarity.

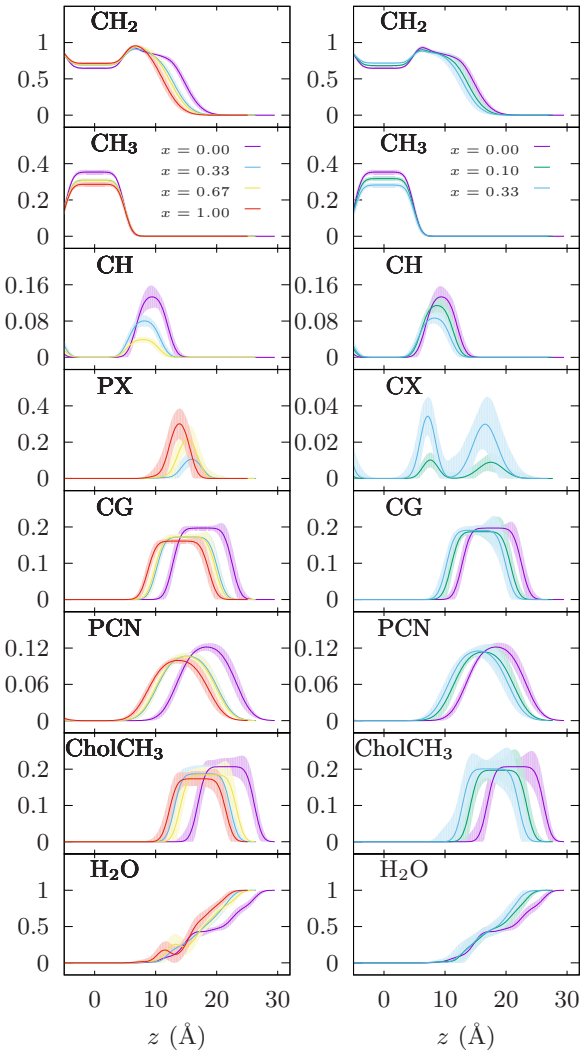

Figure 3: Volume fractions of chemical groups obtained by the analysis of SAXS data for the investigated fractions x of POPC-OOH (left column) and PazePC (right column). Color codes, which refer to the different values of x as shown in the graphs of the CH_3 group, are the same of Figure 2.

Table 2: Parameters obtained by the global-fit analysis of SAXS curves, separated in three classes of fitting parameters and in derived parameters. The unit of length is Å. κ and B and are expressed in 10^{-2} a.u. cm and 10^{-4} a.u., respectively. Validity ranges of fitting parameters: [a] $26.5 \div 28.1$; [b] $327 \div 331$; [c] $29.9 \div 30$; [d] $1.92 \div 1.98$; [e] $0.76 \div 0.84$; [f] $0.38 \div 0.44$; [g] $0.24 \div 0.27$; [h] $3.2 \div 3.7$; [i] $1.7 \div 1.9$; [k] $63.1 \div 85$; [l] $0.94 \div 1$; [m] $1 \div 6$; [n] $1 \div 5$; [o] $0 \div 1$; [p] $1 \div 3$; [q] $0.95 \div 1.05$. [j] Unique fitting value for the curves with $x = 0.00$ of both batches.

First class fitting parameters								
ν_{CH_2}	[a]	28.08±0.03						
V_{PC}	[b]	329.5±0.6						
ν_{H_2O}	[c]	30.00±0.03						
r_{CH_3}	[d]	1.98±0.02						
r_{CH}	[e]	0.83±0.03						
r_{CG}	[f]	0.380±0.004						
r_{PCN}	[g]	0.240±0.009						
Second class fitting parameters								
		$POPC_{1-x}POPC\text{-}OOH_x$				$POPC_{1-x}PazePC_x$		
κ		5.4 ± 0.2				6.7 ± 0.3		
r_X		3.3 ± 0.1[h]				1.88 ± 0.07[i]		
Third class fitting parameters								
x		0.00	0.33	0.67	1.00	0.00	0.10	0.33
A	[k]	65.4±0.4[j]	73±1	73±3	78±2	65.4±0.4[j]	69±1	67±2
x_{pol}	[l]	–	0.95±0.02	0.95±0.02	0.95±0.02	–	0.59±0.04	0.59±0.04
σ_{hyd}	[m]	2.42±0.06[j]	2.44±0.06	2.43±0.07	2.43±0.07	2.42±0.06[j]	2.43±0.06	2.44±0.06
w_{CH_3}	[n]	4.8±0.2[j]	4.9±0.2	4.9±0.2	5.0±0.2	4.8±0.2[j]	4.8±0.2	4.9±0.2
σ_{CH_3}	[m]	1.0±0.1[j]	1.0±0.1	1.0±0.1	1.0±0.1	1.0±0.1[j]	1.0±0.1	1.0±0.1
f_{CH}	[o]	0.65±0.02[j]	0.64±0.02	0.65±0.03	–	0.65±0.02[j]	0.65±0.02	0.65±0.02
w_{CH}	[n]	2.6±0.5[j]	2.6±0.5	2.6±0.5	–	2.6±0.5[j]	2.6±0.5	2.6±0.5
σ_{CH}	[m]	1.11±0.04[j]	1.11±0.04	1.11±0.04	–	1.11±0.04[j]	1.11±0.04	1.10±0.04
$f_{X_{hyd}}$	[o]	–	0.96±0.02	0.97±0.02	0.97±0.02	–	0.57±0.09	0.57±0.09
$w_{X_{hyd}}$	[n]	–	1.9±0.4	1.9±0.4	1.9±0.4	–	1.2±0.4	1.2±0.4
$\sigma_{X_{hyd}}$	[m]	–	1.00±0.04	1.00±0.04	1.00±0.04	–	1.0±0.3	1.0±0.3
f_{CG}	[p]	1.22±0.03[j]	1.20±0.02	1.21±0.06	1.22±0.05	1.22±0.03[j]	1.19±0.02	1.19±0.03
w_{CG}	[n]	4.9±0.2[j]	5.0±0.2	5.0±0.1	5.0±0.1	4.9±0.2[j]	4.9±0.2	4.9±0.3
σ_{CG}	[m]	1.09±0.07[j]	1.09±0.07	1.09±0.07	1.09±0.07	1.09±0.07[j]	1.09±0.07	1.09±0.07
f_{PCN}	[p]	1.27±0.04[j]	1.20±0.03	1.22±0.08	1.22±0.08	1.27±0.04[j]	1.22±0.04	1.22±0.06
w_{PCN}	[n]	4.87±0.04[j]	5.00±0.05	4.99±0.04	5.00±0.03	4.87±0.04[j]	4.98±0.08	5.00±0.09
σ_{PCN}	[m]	2.1±0.3[j]	2.1±0.4	2.1±0.4	2.1±0.4	2.1±0.3[j]	2.1±0.4	2.1±0.4
f_{CholCH_3}	[p]	1.49±0.07[j]	1.40±0.05	1.5±0.1	1.5±0.1	1.49±0.07[j]	1.41±0.07	1.4±0.1
w_{CholCH_3}	[n]	4.6±0.5[j]	4.6±0.5	4.6±0.5	4.6±0.5	4.6±0.5[j]	4.6±0.5	4.6±0.5
σ_{CholCH_3}	[m]	1.0±0.2[j]	1.0±0.2	1.0±0.2	1.0±0.2	1.0±0.2[j]	1.0±0.2	1.0±0.2
$f_{X_{pol}}$	[p]	–	1.26±0.09	1.25±0.08	1.24±0.09	–	1.3±0.2	1.3±0.2
$w_{X_{pol}}$	[n]	–	1.7±0.3	1.7±0.3	1.7±0.3	–	1.6±0.2	1.6±0.2
$\sigma_{X_{pol}}$	[m]	–	1.0±0.4	1.0±0.4	1.0±0.4	–	1.8±0.9	1.8±0.9
d_{H_2O}	[q]	1.042±0.005[j]	1.039±0.002	1.042±0.005	1.042±0.003	1.042±0.005[j]	1.050±0.005	1.049±0.006
B		6.5±0.2	2.7±0.2	4.1±0.3	5.8±0.2	8.4±0.5	18.4±0.9	15.7±0.7
Derived parameters								
χ^2_c		1.04	1.43	1.04	0.54	3.61	0.21	0.43
n_{H_2O}		23±3[j]	30±3	31±4	35±4	23±3[j]	27±3	28±3
$2D_{hyd}$		28.9±0.2[j]	25.3±0.5	24±1	22.4±0.7	28.9±0.2[j]	26.7±0.5	25.3±0.7
D_B		39.0±0.2[j]	35.1±0.6	35±2	33±1	39.0±0.2[j]	36.4±0.6	35.4±0.9
$2D$		59±2[j]	53±2	52±2	50±2	59±2[j]	55±2	54±2

the hydrophobic domain, $r_{CH_3} = \nu_{CH_3}/\nu_{CH_2}$ and $r_{CH} = \nu_{CH}/\nu_{CH_2}$, and in the polar domain, $r_{CG} = \nu_{CG}/V_{PC}$ and $r_{PCN} = \nu_{PCN}/V_{PC}$. To note, according to Kučerka et al. [33], V_{PC} is optmized in a narrow range around 331 Å^3.

Since all curves of the same SAXS experimental campaign have been recorded with the same instrumental configuration, they must be analyzed by exploiting a unique value of the scaling factor κ: hence the first two fitting parameters belonging to the second class are the two scaling factors of the two batches of curves. Other two parameters of this class are the volume ratios $r_X = \nu_X/\nu_{CH_2}$ for PX and CX groups, which cannot vary with mixtures' composition.

We turn now to describe the third class of parameters (curve-specific parameters), reported in the third panels of Table 2. The first free parameters are the areas per lipid unit A, which as described in Materials and Methods allow to derive the monolayer hydrophobic thickness D_{hyd}. The peak positions z_i of all the groups (apart the terminal CH_3 which is fixed at position $z = 0$) are written as $z_i = f_i\, D_{hyd}$, where the true fitting parameter f_i (Table 2) is left to vary between 0 and 1 for the hydrophobic group and from 1 to 3 for the polar groups. The parameter x_{pol}, introduced above, is also left free to vary between 0 and 1. The SLD of the water molecules inside the polar heads is written in terms of its relative mass density, d_{H_2O}, with respect to the bulk water SLD, $\rho_0 = r_e Z_{H_2O}/\nu_{H_2O}$, according to $\rho_N = d_{H_2O}\rho_0$. Best fitting values of d_{H_2O} are searched in the range 0.95-1.05 [45]. The number of hydration water molecules can be derived by $n_{H_2O} = (V - V_{hyd} - V_{pol})/(\nu_{H_2O}/d_{H_2O})$, where $V = D\,A$ is the total hydrated lipid volume.

The validity range of all fitting parameters, reported in the caption of Table 2, has been determined on the basis of updated literature data. The dumping functions F_b for the two batches of SAXS curves have been applied to all the third class parameters reported in Table 2 and their weights have been kept fixed to $\alpha_b = 0.3$.

The goodness of the global-fit is estimated by $\chi^2 = 1.13$, whereas the total weighted damping term has been $\sum_b \alpha_b F_b = 0.12$, corresponding to $\approx 10.3\%$ of χ^2. The best-fitting curves, shown as solid black lines in Figure 2, clearly demonstrate the capability of the MSDP model to reproduce very well the whole SAXS set of experiments. Noteworthy, the global-fit has been carried out by quite important constraint of two unique values of the scaling factors κ (reported in Table 2). This feature, that corresponds to fit data in absolute scale, strongly reduces the space of parameters that can lead to a good fit, providing a further contribution to the robustness of the achieved results. Of note, the groups volume fractions of POPC obtained with the present MSDP model are compared with the ones obtained with the standard SDP model by Kučerka et al. [33] for DOPC at 30°C in Figure S4 of the Supporting Information, revealing a semiquantitative agreement between the two approaches.

The resulting graphs of the volume fractions of all investigated lipid groups are reported in Figure 3. The standard deviations, shown as a colored band around their average values, have been evaluated by 20-fold repeated global-fit procedure. For the oxidized groups (X = PX or X = CX), we report the total volume fraction distribution, $\varphi_X(z) = \varphi_{X_{hyd}}(z) + \varphi_{X_{pol}}(z)$. We also report in in Figure 4 the dependency of the peak position z_i of the volume fraction distribution for each i-group on the composition x of the two mixtures POPC$_{1-x}$POPC-OOH$_x$ (left panel) and POPC$_{1-x}$PazePC$_x$ (right panel). Finally,

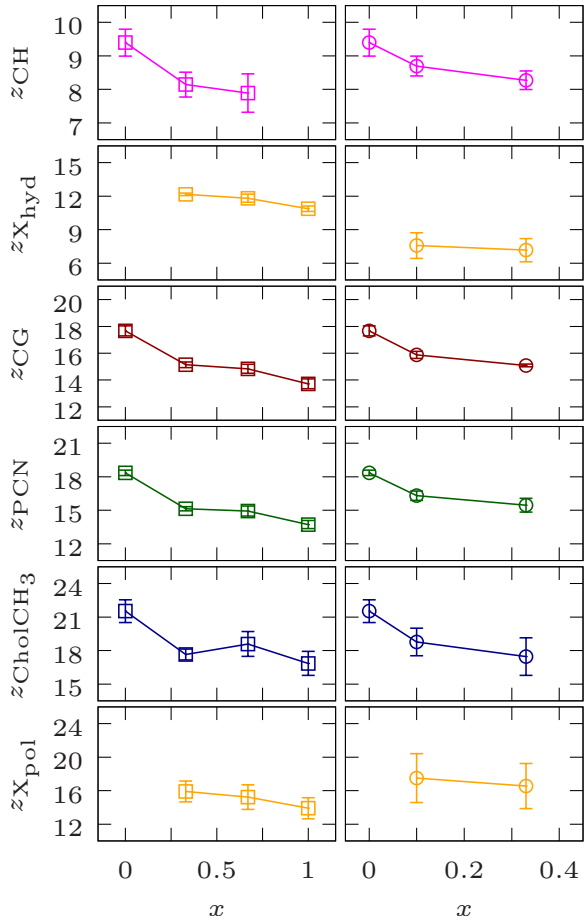

Figure 4: Dependency of the chemical groups peak position z_i on the fraction x of POPC-OOH (left panel) and PazePC (right panel) obtained by the simultaneous fit of the SAXS curves shown in Figure 2. All data are in Å unit. The pedex X represents the PX and the CX groups for the POPC-OOH and the PazePC case, respectively.

the contributions of the volume fractions to the total SLDs are shown as a function of the distance z from the bilayer center in Figure 5.

4. Discussion

It is well known that oxidized lipids impart on membrane structural features. Here we use SAXS technique applied to model lipid bilayers comprising a controlled amount of oxidized species to define their location into the membrane. The strikingly results coming from MSLD/global fit analysis is the fraction x_{pol} of oxidized groups in the polar moiety (Table 2) and their position along the bilayer. In the case of all mixtures of $\mathrm{POPC}_{1-x}\mathrm{POPC\text{-}OOH}_x$ x_{pol} amounts to 0.95 ± 0.02, whereas just 5% of the hydroperoxide group should remain in the hydrophobic medium of the lipid membrane. Note, however, that $f_{\mathrm{PX_{pol}}}$ and $f_{\mathrm{PX_{hyd}}}$ are, on average, 1.26 ± 0.09 and 0.96 ± 0.02, respectively. Therefore, our results give support to infer that 95% of the hydroperoxide groups for each membrane composition reside in the polar

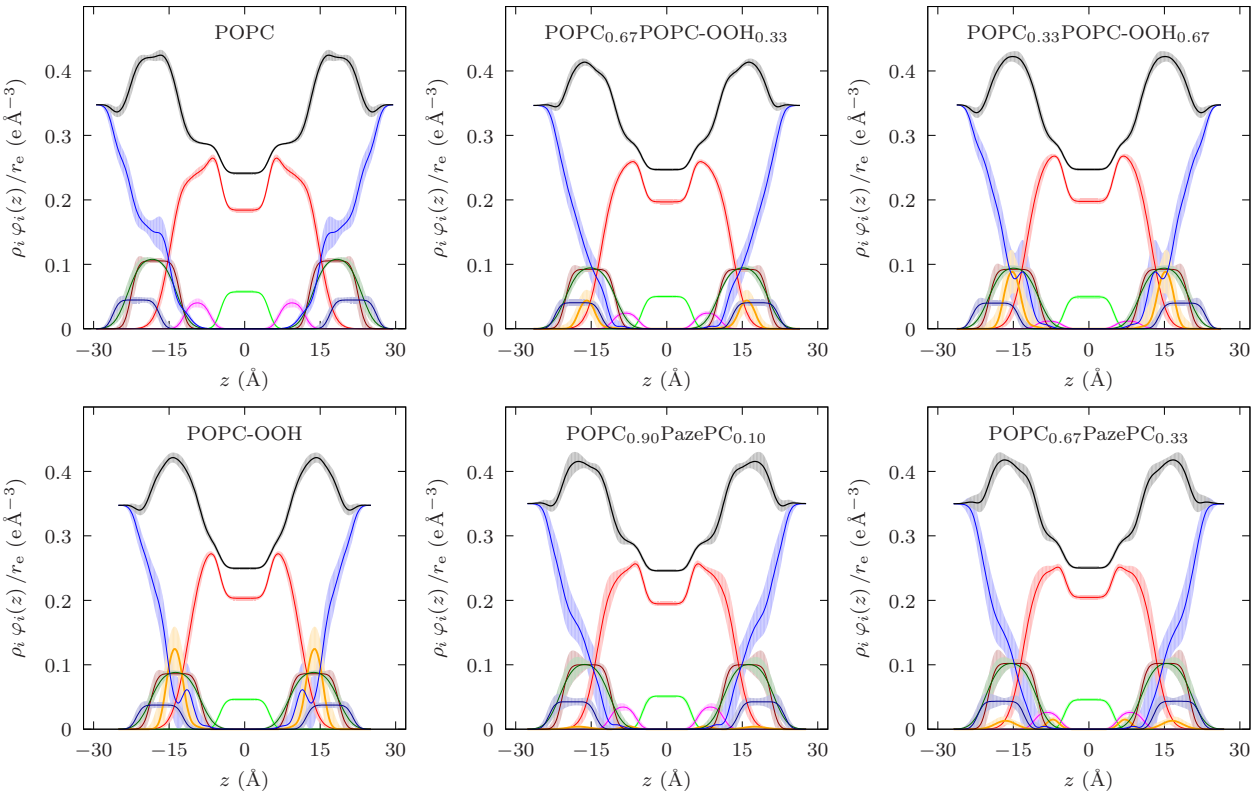

Figure 5: Electron densities of chemical groups obtained by the analysis of SAXS data. Color codes corresponds to CH_2 (red), CH_3 (green), CH (magenta), X (orange), CG (glycerol group $(CH)[(CH_2)(COO)]_2$, dark-red), PCN (phosphate and nitrogen group $(PO_4^-)(CH_2)_2N^+$, dark-green), $CholCH_3$ (metylenes of the choline group $(CH_3)_3$, dark-blue), H_2O (blue). Black lines in the right panel represent the overall electron density, $\rho(z)/r_e$, of the system.

region, whereas 5% lies beneath the polar/apolar interface. In this way, the SAXS results differ from those reported by MD simulations [18] from which a bimodal OOH partition centered in the inner bilayer and at the polar/apolar interface was predicted. The $z_{\mathrm{PX}_{\mathrm{pol}}}$ varies from circa 16 to 14 Å (Figure 3) as the POPC-OOH molar ratio increases from 33 to 100% in the membrane, reminding that $z_{\mathrm{PX}_{\mathrm{pol}}} = f_{\mathrm{PX}_{\mathrm{pol}}} D_{\mathrm{hyd}}$. Note that D_{hyd} (Figure S2 in the Supporting Information) defining the polar/apolar interface decreases from circa 14.5 Å for pure POPC membranes to 11.2 Å for pure POPC-OOH membranes (Table 2). D_{hyd} value found for POPC is in good agreement with data previously reported in the literature [46]. Thus, the observed hydroperoxide group displacement towards smaller z position is due to the overall thinning of the lipid bilayer upon hydroperoxidation. Such observation can also be appreciated on the main features of Figure 3 and Fig 4 in terms of displacements of the CG, PCN and $\mathrm{CholCH_3}$ groups for increasing the POPC-OOH presence in the membrane as well as on the $\mathrm{CH_2}$ group distribution (Figure 3). As a consequence, the layer-to-layer distance between the maximum of electron density taken as the z peak position of the PCN group (Figure 5) is reduced by about 20% (from circa 18 Å to 14 Å as evidenced in Figure 4), with the increase of POPC-OOH amount in the lipid mixture. Accordingly, the membrane thickness decreases as evaluated by D_{hyd} (also on the order of 20%) and by the obtained values of both Luzzati D_B and hydrated D lipid membrane thicknesses (Figure S2, Table 2). It should be remarked that such membrane thinning was recently predicted by MD simulations [1, 18], but to a lesser extent ($\sim$ 10%) than that experimentally revealed by SAXS.

Concomitantly, we also observed an increase in the area A per lipid that varies from 65.4 ± 0.4 Å^2 to 78 ± 2 Å^2 for membranes containing increasing amount of POPC-OOH (Table 2). The latter value is in agreement with that determined by the maximum surface area expansion observed in GUVs under microaspiration procedure [22], and MD predictions [1, 18]. Noteworthy, a perusal of the data regarding z peak position (Figure 4) and volume fraction distribution (Figure 3) of the "extended" hydroperoxide group in respect to the polar groups reveal that the oxidized specie must be preferentially located near the CG and PCN groups. Moreover, the remaining 5% of hydroperoxide groups also reside near the polar/apolar interface. According to Garrec et al. [19], the hydroperoxide groups form 4-times more hydrogen bonds with carbonyls than with phosphates, but they have a higher propensity to form hydrogen bonds with water beneath the head group. Here, we clearly determine that OOH group mainly resides near the CG and PCN moieties with a very small fraction beneath the polar/apolar interface, resulting in practically an unimodal OOH group volume fraction displayed in Figure 3.

Regarding the mixture $\mathrm{POPC}_{1-x}\mathrm{PazePC}_x$, the value of x_{pol} that describes the partitioning of the carboxylate group CX is 0.59 ± 0.04, indicating that a significant fraction of it is in the hydrophobic part of the lipid. However, the z position of $\mathrm{CX}_{\mathrm{pol}}$ (Figure 3 and Figure 4) highlights the fact that, similarly to hydroperoxide, the carboxyl group has affinity to CG and PCN groups, whereas the z position of $\mathrm{CX}_{\mathrm{hyd}}$ is in the middle of the hydrophobic border, $f_{\mathrm{CX}_{\mathrm{hyd}}} = 0.57 \pm 0.09$. These features can be also appreciated by the inspection of Figure 3 where a bimodal volume distribution of the carbonyl group is clearly seen . The

overall picture the emerges is that the CX group is in a dynamic movement across the apolar/polar border. Using MD simulations Khandelia and Mouritsen [27] observed that the truncated chain of PazePC can reverse its orientation, thus exposing the carboxyl group to water phase. The CX partition between hydrophilic and hydrophobic regions was dependent on oxidized group concentration. Unlikely, here we show that the CX partition is the same for POPC lipid bilayers containing up to 33 mol % of PazePC. Noteworthy, although the values of D_{hyd}, $D_B/2$ and D are equal to those observed for $\mathrm{POPC}_{1-x}\mathrm{POPC\text{-}OOH}_x$ membranes with $x = 0.33$, thus also indicating a membrane thinning upon oxidation, the area increase is significantly smaller: 73 ± 3 Å^2 and 67 ± 2 Å^2 (Table 2) for membranes containing 33% of POPC-OOH and PazePC, respectively. Therefore, the molecular geometry of the oxidized product plays a key role in the molecular area available per lipid. The number of water molecules in the polar domain, $\mathrm{n_{H_2O}}$ (Table 2), in all cases found with a mass density $\approx 4\%$ higher than the mass density of bulk water molecules, has also been determined. Of note, the higher is A the higher is $\mathrm{n_{H_2O}}$, indicating that the overall increase of the A and the parallel decrease of D in all cases leave a greater available space for accommodating water. It should be noticed, however, that the oxidation does not promote a deeper water penetration in the membrane interior in respect to POPC bilayers (Figure 3). Such an observation is in complete agreement with no change in permeability by exchanging POPC by POPC-OOH in GUVs experiments [22]. On other hand, changes in permeability is expected in the case of membranes containing shortened tails oxidized lipids [26, 24, 25] but not observed here. However, increase in permeability must depend on the oxidation level as previously reported by Lis et al. [47] for PazePC: at 15-30% oxidation, only individual water molecules spontaneously permeated across the bilayer, whereas at 55-66% oxidation, water clusters originating from water defects in the headgroup region can cross the bilayer.

5. Conclusion

In the current work, we assess the effect of lipid oxidization on the structural properties of model membranes in a quantitative manner. By controlling the amount of oxidized lipids in the membrane, we investigate POPC LUVs in the absence and presence of two different OxLs, PazePC with a carboxyl group hanging in a truncated alky chain and POPC-OOH with a hydroperoxide group linked to C9−C10 atom of the unsaturated alkyl tail. The electron density profile (Figure 5) was retrieved from the SAXS data analysis by taking into account the scattering of each chemical group of the lipid molecules. It is noteworthy that the hydroperoxide group preferentially resides in the membrane polar moiety, close to carbonyl and phosphate groups, probably forming H-bonds. The presence of hydroperoxide groups promotes a decrease in membrane thickness accompanied by an increase in area per lipid. Indeed, the area per polar head, A, of pure POPC obtained by the global-fit is 65.4 ± 0.4 Å^2, in very good agreement with the value of 65.2 Å^2 obtained by the Molecular Dynamics study of Gurtovenko and Vattulainen [48]. By increasing the fraction x of POPC-OOH, A increases up to the value 78 ± 2 Å^2 for $x = 1$ and, in parallel, the overall thickness of the membrane, estimated by different parameters, decreases: the hydrophobic thickness $2D_{\mathrm{hyd}}$ changes from 28.9 ± 0.2 Å to 22.4 ± 0.7 Å, the Luzzati thickness D_B from 39.0 ± 0.2 Å to

33±1 Å and the overall hydrated lipid thickness $2D$ from 59±2 Å to 50±2 Å. The relationship between oxidation and increase of area had already been verified in previous works using GUVs [20, 22]. On the other hand, the decrease in the lipid bilayer due to oxidation is here experimentally verified for the first time. Results for the PazePC series, investigated up to the fraction $x = 0.33$, are different from those obtained for POPC-OOH: the carboxyl group presents a bimodal distribution in the hydrophilic and hydrophobic regions, probably due to a dynamic movement of the shortened alkyl tail towards the polar region. The area A slightly increases up to 67 ± 2 Å^2, certainly reflecting the peculiar PazePC molecular geometry. The three thicknesses $2D_{\mathrm{hyd}}$, D_B and $2D$ decrease to 25.3 ± 0.7 Å, 35.4 ± 0.9 Å and 54 ± 2 Å, respectively, in good agreement with the small bilayer thickness variation observed by Makky and Tanaka [29] for systems composed of POPC with 20% of PazePC deposited onto a substrate. In summary, it has been here demonstrated that the application of the MSLD model to analyze SAXS data consents to experimentally unveil the location of oxidized groups inside the lipid membrane, which allows for obtaining important parameters regarding membrane structural features.

Acknowledgments

This work was supported by São Paulo Research Foundation (FAPESP) (Process 2012/50680-5). R. R. and F. S. thank the PhD and invited professor fellowships supported by FAPESP (2014/02511-5 and 2016/25847-4, respectively). R. I. is the recipient of The National Council for Scientific and Technological Development (CNPq, Brazil) research fellowship. The authors would also like to thank the LNLS/CNPEM-ABTLuS (Campinas, Brazil) for the use of SAXS beamline, H. C. Junqueira (Institute of Chemistry, University of Sao Paulo, SP, Brazil) for preparing POPC-OOH and L. G. Dias (FFCLRP-USP) for helpful discussions.

Appendix A. Supplementary data

Supplementary data to this article can be found online at ....

References

[1] P. Siani, R. M. de Souza, L. G. Dias, R. Itri, H. Khandelia, An overview of molecular dynamics simulations of oxidized lipid systems, with a comparison of ELBA and MARTINI force fields for coarse grained lipid simulations, BBA - Biomembranes 1858 (2016) 2498–2511.

[2] A. Catalá, Lipid peroxidation of membrane phospholipids generates hydroxy-alkenals and oxidized phospholipids active in physiological and/or pathological conditions, Chemistry and Physics of Lipids 157 (2009) 1–11.

[3] G. L. Nicolson, M. E. Ash, Lipid Replacement Therapy: A natural medicine approach to replacing damaged lipids in cellular membranes and organelles and restoring function, BBA - Biomembranes 1838 (2014) 1657 – 1679.

[4] G. Spiteller, The relation of lipid peroxidation processes with atherogenesis: A new theory on atherogenesis, Mol. Nutr. Food Res. 49 (2005) 999 – 1013.

[5] G. O. Fruhwirth, A. Loidl, A. Hermetter, Oxidized phospholipids: From molecular properties to disease, BBA - Molecular Basis of Disease 1772 (2007) 718 – 736.

[6] N. A. Strobel, R. G. Fassett, S. A. Marsh, J. S. Coombes, Oxidative stress biomarkers as predictors of cardiovascular disease, International Journal of Cardiology 147 (2011) 191 – 201.
[7] F. H. Greig, S. Kennedy, C. M. Spickett, Physiological effects of oxidized phospholipids and their cellular signaling mechanisms in inflammation, Free Radical Biology and Medicine 52 (2012) 266 – 280.
[8] R. Volinsky, P. K. J. Kinnunen, Oxidized phosphatidylcholines in membrane-level cellular signaling: from biophysics to physiology and molecular pathology, FEBS Journal 280 (2013) 2806 –2816.
[9] S. Pope, J. M. Land, S. J. R. Heales, Oxidative stress and mitochondrial dysfunction in neurodegeneration; cardiolipin a critical target?, BBA - Bioenergetics 1777 (2008) 794 – 799.
[10] H. Mitomo, W.-H. Chen, S. L. Regen, Oxysterol-Induced Rearrangement of the Liquid-Ordered Phase: A Possible Link to Alzheimers Disease?, JACS 131 (2009) 12354 – 12357.
[11] T. Farooqui, A. A. Farooqui, Lipid-Mediated Oxidative Stress and Inflammation in the Pathogenesis of Parkinson's Disease, Parkinson's Disease 2011 (2001) 247467–247476.
[12] E. Niki, Lipid peroxidation: Physiological levels and dual biological effects, Free Radical Biology and Medicine 47 (2009) 469 – 484.
[13] P. K. Kinnunen, K. Kaarniranta, A. K. Mahalka, Protein-oxidized phospholipid interactions in cellular signaling for cell death: From biophysics to clinical correlations, BBA - Biomembranes 1818 (2012) 2446 – 2455.
[14] A. W. Girotti, T. Kriska, Role of Lipid Hydroperoxides in Photo-Oxidative Stress Signaling, Antioxidants & Redox Signaling 6 (2004) 301 – 310.
[15] R. Itri, H. C. Junqueira, O. Mertins, M. S. Baptista, Membrane changes under oxidative stress: the impact of oxidized lipids, Biophysical Reviews 6 (2014) 47–61.
[16] P. Jurkiewicz, A. Olyska, L. Cwiklik, E. Conte, P. Jungwirth, F. M. Megli, M. Hof, Biophysics of lipid bilayers containing oxidatively modified phospholipids: Insights from fluorescence and {EPR} experiments and from {MD} simulations, Biochimica et Biophysica Acta (BBA) - Biomembranes 1818 (2012) 2388–2402.
[17] J. Wong-ekkabut, Z. Xu, W. Triampo, I.-M. Tang, D. P. Tieleman, L. Monticelli, Effect of Lipid Peroxidation on the Properties of Lipid Bilayers: A Molecular Dynamics Study, Biophysical Journal 93 (2007) 4225–4236.
[18] Y. Guo, V. A. Baulin, F. Thalmann, Peroxidised phospholipid bilayers: insight from coarse-grained molecular dynamics simulations, Soft Matter 12 (2016) 263–271.
[19] J. Garrec, A. Monari, X. Assfeld, L. M. Mir, M. Tarek, Lipid Peroxidation in Membranes: The Peroxyl Radical Does Not Float, The Journal of Physical Chemistry Letters 5 (2014) 1653–1658.
[20] K. A. Riske, T. P. Sudbrack, N. L. Archilha, A. F. Uchoa, A. P. Schroder, C. M. Marques, M. S. Baptista, R. Itri, Giant Vesicles under Oxidative Stress Induced by a Membrane-Anchored Photosensitizer, Biophysical Journal 97 (2009) 1362–1370.
[21] S. Sankhagowit, S.-H. Wu, R. Biswas, C. T. Riche, M. L. Povinelli, N. Malmstadt, The dynamics of giant unilamellar vesicle oxidation probed by morphological transitions, BBA - Biomembranes 1838 (2014) 2615 – 2624.
[22] G. Weber, T. Charitat, M. S. Baptista, A. F. Uchoa, C. Pavani, H. C. Junqueira, Y. Guo, V. A. Baulin, R. Itri, C. M. Marques, A. P. Schroder, Lipid oxidation induces structural changes in biomimetic membranes, Soft Matter 10 (2014) 4241–4247.
[23] C. K. Haluska, M. S. Baptista, A. U. Fernandes, A. P. Schroder, C. M. Marques, R. Itri, Photo-activated phase separation in giant vesicles made from different lipid mixtures, BBA - Biomembranes 1818 (2012) 666 – 672.
[24] J. Heuvingh, S. Bonneau, Asymmetric Oxidation of Giant Vesicles Triggers Curvature-Associated Shape Transition and Permeabilization, Biophysical Journal 97 (2009) 2904 – 2912.
[25] K. A. Runas, N. Malmstadt, Low levels of lipid oxidation radically increase the passive permeability of lipid bilayers, Soft Matter 11 (2015) 499–505.
[26] W. Caetano, P. S. Haddad, R. Itri, D. Severino, V. C. Vieira, M. S. Baptista, A. P. Schrder, C. M. Marques, Photo-Induced Destruction of Giant Vesicles in Methylene Blue Solutions, Langmuir 23 (2007) 1307–1314.

[27] H. Khandelia, O. G. Mouritsen, Lipid Gymnastics: Evidence of Complete Acyl Chain Reversal in Oxidized Phospholipids from Molecular Simulations, Biophysical Journal 96 (2009) 2734 – 2743.
[28] J.-P. Mattila, K. Sabatini, P. K. J. Kinnunen, Oxidized phospholipids as potential molecular targets for antimicrobial peptides, BBA - Biomembranes 1778 (2008) 2041 – 2050.
[29] A. Makky, M. Tanaka, Impact of Lipid Oxidization on Biophysical Properties of Model Cell Membranes, The Journal of Physical Chemistry B 119 (18) (2015) 5857–5863.
[30] S. S. Davies, A. V. Pontsler, G. K. Marathe, K. A. Harrison, R. C. Murphy, J. C. Hinshaw, G. D. Prestwich, A. S. Hilaire, S. M. Prescott, G. A. Zimmerman, T. M. McIntyre, Oxidized Alkyl Phospholipids Are Specific, High Affinity Peroxisome Proliferator-activated Receptor Ligands and Agonists, J. Biol. Chem. 276 (2001) 16015 – 16023.
[31] H. I. Petrache, S. E. Feller, J. F. Nagle, Determination of component volumes of lipid bilayers from simulations, Biophys. J. 72 (1997) 2237–2242.
[32] J. B. Klauda, N. Kučerka, B. R. Brooks, R. W. Pastor, J. F. Nagle, Simulation-Based Methods for Interpreting X-Ray Data from Lipid Bilayers, Biophys. J. 90 (2006) 2796–2807.
[33] N. Kučerka, J. F. Nagle, J. N. Sachs, S. E. Feller, J. Pencer, A. Jackson, J. Katsaras, Lipid Bilayer Structure Determined by the Simultaneous Analysis of Neutron and X-Ray Scattering Data, Biophys. J. 95 (2008) 2356–2367.
[34] N. Kučerka, M.-P. Nieh, J. Katsaras, Fluid phase lipid areas and bilayer thicknesses of commonly used phosphatidylcholines as a function of temperature, BBA - Biomembranes 1808 (2011) 2761–2771.
[35] P. Heftberger, B. Kollmitzer, F. A. Heberle, J. Pan, M. Rappolt, H. Amenitsch, N. Kučerka, J. Katsaras, G. Pabst, Global small-angle X-ray scattering data analysis for multilamellar vesicles: the evolution of the scattering density profile model, J. Appl. Crystallogr. 47 (2014) 173–180.
[36] J. Pan, X. Cheng, M. Sharp, C.-S. Ho, N. Khadka, J. Katsaras, Structural and mechanical properties of cardiolipin lipid bilayers determined using neutron spin echo, small angle neutron and X-ray scattering, and molecular dynamics simulations, Soft Matter 11 (2015) 130–138.
[37] F. Spinozzi, C. Ferrero, M. G. Ortore, A. D. M. Antolinos, P. Mariani, GENFIT: software for the analysis of small-angle X-ray and neutron scattering data of macromolecules in-solution, J. App. Cryst. 47 (2014) 1132–1139.
[38] C. Kawai, J. C. Ferreira, M. S. Baptista, I. L. Nantes, Not Only Oxidation of Cardiolipin Affects the Affinity of Cytochrome c for Lipid Bilayers, The Journal of Physical Chemistry B 118 (41) (2014) 11863–11872.
[39] J. Pan, X. Cheng, F. A. Heberle, B. Mostofian, N. Kučerka, P. Drazba, J. Katsaras, Interactions between Ether Phospholipids and Cholesterol As Determined by Scattering and Molecular Dynamics Simulations, J. Phys. Chem. B 116 (2012) 14829–14838.
[40] O. Glatter, Fourier Transformation and Deconvolution, in: P. Lindner, T. Zemb (Eds.), Neutron, X-rays and Light. Scattering Methods Applied to Soft Condensed Matter, North-Holland, 103–124, 2002.
[41] F. Spinozzi, P. Mariani, L. Paccamiccio, L. Q. Amaral, New Lamellar Phase With Pores in the Chain-Melting Regime of an Anionic Phospholipid Dispersion, J. Phys.: Conf. Ser. 247 (2010) 012019.
[42] D. Marsh, Molecular volumes of phospholipids and glycolipids in membranes, Chem. Phys. Lipids 163 (2010) 667 – 677.
[43] O. Glatter, O. Kratky, Small Angle X-Ray Scattering, Academic Press, ISBN 0-12-286280-5, 1982.
[44] F. Spinozzi, R. Itri, Small-angle scattering of stacks of large bilayers with cylindrically shaped defects, In preparation .
[45] F. Spinozzi, L. Q. Amaral, Pore Model in the Melting Regime of a Lyotropic Biomembrane with an Anionic Phospholipid, Langmuir 32 (2016) 13556–13565.
[46] N. Kučerkaa, van B. Oosten, J. Pan, F. A. Heberle, , T. A. Harroun, J. Katsaras, Molecular Structures of Fluid Phosphatidylethanolamine Bilayers Obtained from Simulation-to-Experiment Comparisons and Experimental Scattering Density Profiles, The Journal of Physical Chemistry B 119 (2015) 1947–1956.
[47] M. Lis, A. Wizert, M. Przybylo, M. Langner, J. Swiatek, P. Jungwirth, L. Cwiklik, The effect of lipid oxidation on the water permeability of phospholipids bilayers, Phys. Chem. Chem. Phys. 13 (2011) 17555–17563.

[48] A. A. Gurtovenko, I. Vattulainen, Effect of NaCl and KCl on Phosphatidylcholine and Phosphatidylethanolamine Lipid Membranes: Insight from Atomic-Scale Simulations for Understanding Salt-Induced Effects in the Plasma Membrane, J. Phys. Chem. B 112 (2008) 1953–1962.